Backbone Dynamics of Plastocyanin in Both Oxidation States

SOLUTION STRUCTURE OF THE REDUCED FORM AND COMPARISON WITH THE OXIDIZED STATE*[S]

Ivano Bertini‡, Donald A. Bryant§, Stefano Ciurli¶‖, Alexander Dikiy¶, Claudio O. Fernández‡**‡‡, Claudio Luchinat§§, Niyaz Safarov¶, Alejandro J. Vila¶¶, and Jindong Zhao§‖

From the ‡Magnetic Resonance Center and Department of Chemistry, University of Florence, Via L. Sacconi, 6-50019 Sesto Fiorentino, Italy, the §Department of Biochemistry and Molecular Biology, the Pennsylvania State University, University Park, Pennsylvania 16802, the ¶Department of Agro-Environmental Science and Technology, University of Bologna, Viale Berti Pichat 10, 40127 Bologna, Italy, **LANAIS RMN 300 (CONICET-UBA), Junin 956, 1113 Buenos Aires, Argentina, §§Magnetic Resonance Center and Department of Agricultural Biotechnology, University of Florence, Via L. Sacconi, 6-50019 Sesto Fiorentino, Italy, and ¶¶Biophysics Section, Department of Biological Chemistry, University of Rosario, Suipacha 531, 2000 Rosario, Argentina

A model-free analysis based on ^{15}N R_1, ^{15}N R_2, and ^{15}N-^1H nuclear Overhauser effects was performed on reduced (diamagnetic) and oxidized (paramagnetic) forms of plastocyanin from *Synechocystis* sp. PCC6803. The protein backbone is rigid, displaying a small degree of mobility in the sub-nanosecond time scale. The loops surrounding the copper ion, involved in physiological electron transfer, feature a higher extent of flexibility in the longer time scale in both redox states, as measured from D_2O exchange of amide protons and from NH-H_2O saturation transfer experiments. In contrast to the situation for other electron transfer proteins, no significant difference in the dynamic properties is found between the two redox forms. A solution structure was also determined for the reduced plastocyanin and compared with the solution structure of the oxidized form in order to assess possible structural changes related to the copper ion redox state. Within the attained resolution, the structure of the reduced plastocyanin is indistinguishable from that of the oxidized form, even though small chemical shift differences are observed. The present characterization provides information on both the structural and dynamic behavior of blue copper proteins in solution that is useful to understand further the role(s) of protein dynamics in electron transfer processes.

Plastocyanins are copper-containing electron transfer pro-

teins that shuttle electrons between the reduced cytochrome *f* of the membrane-bound b_6f complex and the photo-oxidized chlorophyll special pair $P700^+$ of photosystem I during oxygenic photosynthesis in green algae, higher plants, and cyanobacteria (1–4). In plastocyanins, the Cu(II)/Cu(I) ion resides in the so-called type I copper center, characterized by the presence of one cysteine and two histidine residues strongly bound to copper in a trigonal plane (5–7). A weakly bound methionine sulfur atom completes the distorted coordination geometry of the metal ion (8).

The electron transfer mediated by plastocyanin exhibits distinctive features in different organisms (2). Plastocyanin is the only soluble electron carrier between cytochrome b_6f and photosystem I in higher plants (4). Depending on the organism and the copper levels in the growth medium, cytochrome c_6 can replace plastocyanin in some cyanobacteria and most eukaryotic algae (9, 10).

Molecular recognition between plastocyanins and their redox partners has been thoroughly studied in plants, even if some aspects are still obscure. Two conserved surface regions have been identified on plastocyanin: the so-called "eastern" and "northern" protein patches (2, 11). The eastern patch is a negatively charged region, conserved in plant plastocyanins, whereas a hydrophobic surface around the redox metal center constitutes the so-called northern pole (2, 11). The charged region participates in electrostatic interactions with the electron transfer partners, whereas the hydrophobic patch is involved in electron transfer through the copper-bound His[86]. In plastocyanins from cyanobacteria, the negatively charged patch is significantly smaller than in proteins from higher plants (2, 12–14); however, the hydrophobic patch is still present and is physiologically relevant (15).

Plastocyanins have been subjected to thorough structural characterization. NMR or x-ray structures of proteins from 14 different biological sources are available (12, 13, 16–29). Some of us have recently reported (29) the first solution structure of an oxidized plastocyanin, from *Synechocystis* sp. PCC6803, which was used to assess the level of refinement attainable for an NMR solution structure of a copper(II)-containing protein. The present study reports on the backbone mobility of both redox forms of plastocyanin, spanning a wide range of time scales, as well as an investigation of the H_2O/D_2O exchange in different time frames. Mobility studies are so far available for two blue copper proteins, azurin (30) and pseudoazurin (31), in the reduced form. The mobility of cupredoxins in their oxidized form has never been studied by NMR due to the difficulties

related to the presence of the strongly paramagnetic Cu(II) ion. The structure of the reduced plastocyanin is also reported, together with a thorough comparison with the solution structure of the oxidized form.

EXPERIMENTAL PROCEDURES

Cloning of Synechocystis sp. PCC6803 Plastocyanin Gene in Escherichia coli—The *petE* gene encoding plastocyanin was amplified from total genomic DNA isolated from the cyanobacterium *Synechocystis* sp. PCC6803 by polymerase chain reaction using the following primers: 5′-CCCCGCTG**CCATGG**CCAATGCAACA-3′; 5′-CGACACACA**AGATC**TAGCTGGCTGAT-3′.

These primers introduced a methionine start codon (bold type) as well as an *Nco*I site (underlined) at the 5′-end of the coding sequence of mature plastocyanin and a *Bgl*II site (underlined) downstream from the stop codon of the gene. A polymerase chain reaction product with the expected size and containing the expected *Hin*dIII site was amplified. The product was digested with *Nco*I and *Bgl*II and cloned into plasmid pET3d that had been digested with *Nco*I and *Bam*HI to produce plasmid pET3d::6803 *petE*. It should be noted that this construction is expected to cause the production of a protein whose N-terminal sequence after processing of the N-terminal methionine residue is ANATVKMGSD. . . . This N-terminal sequence corresponds to that of the wild-type protein (32). Nucleotide sequence analysis of plasmid pET3d::6803 *petE* revealed that the expressed protein would contain a single amino acid difference from the published wild-type sequence. The GAG codon encoding the carboxyl-terminal glutamic acid was found to be GAC encoding aspartic acid. It is not known whether this change resulted from a mutation introduced by the *Taq* polymerase used in the polymerase chain reaction amplification or whether this change had occurred in the laboratory *Synechocystis* sp. PCC6803 strain used to produce the genomic DNA. The resultant expression plasmid was transformed into *E. coli* strain BL21(DE3)pLysS for overproduction of the PetE protein as subsequently described.

Protein Expression and Purification—The expression of *Synechocystis* sp. PCC 6803 plastocyanin in *E. coli* was based on the T7 expression system described by Studier *et al.* (33). *E. coli* BL21(DE3)pLysS cells transformed by plasmid pET3d::6803 *petE* were grown at 37 °C in 1 liter of Luria broth (10 g of bactotryptone, 5 g of yeast extract, 10 g of NaCl per liter) supplemented with ampicillin (50 μg ml^{-1}) and chloramphenicol (34 μg ml^{-1}) in shaking flasks at 37 °C until the A_{600} = 0.6–1.0 (~3 h). ^{15}N-Enriched plastocyanin was obtained from cells grown as described above, but in mineral medium containing 6 g of Na$_2$HPO$_4$, 3 g of KH$_2$PO$_4$, 0.5 g of NaCl, 1.25 g of [^{15}N](NH$_4$)$_2$SO$_4$, 1 mM MgSO$_4$, 20 g glucose, 50 mg of ampicillin, and 34 mg chloramphenicol per liter.

The cells were collected and resuspended in the same volume of freshly prepared medium. Isopropyl- β-D-thiogalactopyranoside and CuSO$_4$ were added to a final concentration of 0.4 and 0.1 mM, respectively, for induction of plastocyanin expression. The cells were harvested by centrifugation after 3–4 h of additional growth and resuspended in 50 mM Tris-HCl buffer, pH 7.8 (1/10 culture volume).

The cell suspension was subjected to 3 cycles of freezing at −80 °C and thawing. Membrane fragments and cell debris were removed by centrifugation at 10,000 × *g* for 40 min, and the clear extract was incubated with DNase I (Fluka) from bovine pancreas (20 mg l^{-1}) and MgCl$_2$ (10 mM) for 30 min at room temperature in order to digest chromosomal DNA. The obtained extract was used for subsequent purification.

Solid (NH$_4$)$_2$SO$_4$ was added to the extract to a final concentration of 2 M, and the insoluble material was removed by centrifugation at 10,000 × *g* for 30 min. The clear supernatant was loaded on a phenyl-Sepharose hydrophobic interaction column (2.6 × 20 cm), and a gradient of (NH$_4$)$_2$SO$_4$ (from 2 to 0 M) in 20 mM Tris-HCl buffer, pH 7.3, was used to fractionate the extracted proteins. Two plastocyanin peaks (oxidized and reduced forms) were separately eluted. These fractions were pooled, dialyzed against 20 mM Tris-HCl buffer, pH 7.3, using a membrane with a molecular weight cut-off of 3 kDa and concentrated to 2 ml using an Amicon ultrafiltration unit equipped with a YM3 membrane. The concentrated protein fraction was loaded onto a Superdex 75 size-exclusion column (2.6 × 60 cm) equilibrated with 20 mM Tris-HCl buffer, pH 7.3, containing 200 mM NaCl. The eluted plastocyanin fractions were pooled and concentrated, and (NH$_4$)$_2$SO$_4$ was added to the final concentration of 2 M.

The final purification step was performed with a hydrophobic interaction, alkyl-Sepharose HR 10/10 column (Amersham Pharmacia Biotech), using a gradient of (NH$_4$)$_2$SO$_4$ (from 2 to 1 M) in 20 mM Tris-HCl

buffer, pH 7.3, to elute the plastocyanin. The pooled plastocyanin fractions (20–25 mg of purified protein from 1 liter of cell culture) were homogenous as judged by SDS-PAGE carried out using a 16% acrylamide separating gel and a Bio-Rad Miniprotean apparatus (Richmond, CA). The absorbance ratio (A_{278}/A_{600}) of the oxidized plastocyanin in the final preparation was 2.0, as reported earlier for native *Synechocystis* sp. PCC6803 plastocyanin (32). The protein concentration of crude preparations was determined using the extinction coefficient of 4.5 × 10^{-3} M^{-1} cm^{-1} at 600 nm (32, 34). The total protein concentration in the final fraction was determined by the method of Bradford (35) using bovine serum albumin as a standard.

NMR Spectroscopy Data Acquisition and Processing—Samples for NMR spectroscopy (2–3 mM) were prepared in 50 mM sodium phosphate buffer (either in 90% H$_2$O, 10% D$_2$O or in 100% D$_2$O) at pH 5.2–6.5. Complete reduction of the protein was obtained by addition of a slight excess of a freshly prepared sodium ascorbate solution, and the sample was kept under argon during the NMR experiments. The oxidation was achieved using a slight excess of ferricyanide, subsequently removed by gel filtration. A catalytic amount of laccase was then added to the oxidized protein sample, which was kept under oxygen throughout the NMR experiments.

Bruker Avance spectrometers operating at 800, 700, 600, and 500 MHz proton Larmor frequencies were used to collect NMR spectra. Data acquisition and processing were performed using a standard Bruker software package (XWINNMR).

NMR Assignment and Structure Determination—The acquisition of homonuclear and heteronuclear NMR spectra, as well as data processing, were performed using the same strategy as described previously (29). The time settings in the pulse sequences were largely coincident with those used to detect diamagnetic connectivities in the case of the oxidized form of the protein (29). The program XEASY (36) was employed for spectral analysis and for cross-peaks integration. The sequence-specific resonance assignment was carried out using standard procedures (37, 38).

The volumes of NOESY[1] cross-peaks, together with the values of $^3J_{\text{H}\alpha\text{-NH}}$ coupling constants from three-dimensional HNHA experiments (39), and in combination with some hydrogen bonds constraints, were utilized for structure calculation of the reduced protein, using the DYANA package (40). Additional ϕ and ψ dihedral angles constraints were obtained from the relative intensities of the intra- and inter-residue Hα-NH NOESY cross-peaks as measured in NOESY-heteronuclear multiple quantum coherence and NOESY spectra (41). The constraints for the copper atom were treated as described previously (29).

The structure calculation followed closely the procedure described for the oxidized protein (29). The 35 structures with the lowest target function obtained from DYANA calculations (42) were selected as a single family for further analysis. The mean structure from the DYANA family was calculated using MOLMOL (43) and subjected to restrained energy minimization using the SANDER module of the AMBER 5.0 program package (44). The quality of the structures was determined using PROCHECK (45). The coordinates of the structure family and the minimized DYANA mean structure have been deposited in the Protein Data Bank.

NMR Experiments Aimed at Determining Backbone Protein Mobility in the Sub-nanosecond Time Scale—The protein mobility in this time range was studied in both reduced and oxidized plastocyanin at 295 K and pH 6.50. ^{15}N nuclear spin relaxation experiments were recorded at 600.13 (^{1}H) and 60.81 MHz (^{15}N) on a Bruker Avance 600 NMR spectrometer. All spectra were recorded with a spectral width of 6614 Hz over 2048 real data points in ω2, and the carrier frequency was set at the H$_2$O signal frequency. The time proportional phase incrementation method was used for frequency discrimination in ω1 (46). The spectral width in ω1 was 2068 Hz, sampled over 256 real t_1 points, and 8 transients (32 for heteronuclear NOE experiments) were acquired per each t_1 point. The recycle delay was 1.7 s (3.0 s for heteronuclear NOE). Suppression of the intense water resonance was accomplished by the use of a water-selective inversion pulse train (WATERGATE) (47) together with a flip-back pulse (48). All spectra were transformed with 1 × 1024 points in the *F*2 and *F*1 dimensions, respectively. Only the downfield part of the ^{1}H spectra containing the H-N connectivities (5–12 ppm) was kept for the data analysis. The cross-peaks were integrated using the standard routine of the XWINNMR program.

---

[1] The abbreviations used are: NOESY, nuclear Overhauser effect spectroscopy; NOE, nuclear Overhauser effect; r.m.s.d., root mean square deviation; CPMG, Carr-Purcell-Meiboom-Gill.

^{15}N longitudinal relaxation rate (R_1) values were measured as described previously (49). The recovery delays used in the pulse sequence were 5, 10, 20, 40, 80, 150, 300, 500, 750, 1000, 1500, 2000, and 2250 ms. ^{15}N R_2 rates were measured using the CPMG pulse sequence with a refocusing delay of 450 μs (49, 50). Fifteen experiments with recovery delays of 7, 14, 22, 29, 43, 57, 72, 86, 100, 129, 158, 172, 215, 244, and 287 ms were collected. Heteronuclear ^{1}H-^{15}N NOE experiments were measured using a described pulse sequence (48). Two spectra were collected, one with proton saturation and one without. Saturation of the proton spectrum was achieved by applying non-selective pulses during the recycle delay. The heteronuclear NOE values were obtained as the ratio of the intensity measured with and without saturation of the amide protons. The uncertainties in the NOE values, expressed as 3σ, were estimated by collecting two independent data sets. Relaxation rates R_1 and R_2 were determined by fitting the cross-peak intensities (I), measured as a function of the variable delay (t) within the pulse sequence to a single exponential decay by using the Levenberg-Marquardt algorithm (51, 52) according to the following equation: $I(t) = A + B \cdot \exp(-Rt)$. A, B, and R were adjustable fitting parameters. For R_2, A was set equal to 0 in the fitting procedure. Uncertainties in the R_1 and R_2 values were determined by using a Monte Carlo approach (53–55).

Hydrodynamic calculations were performed using the program Quadric Diffusion 1.11 (56) applied to the energy-minimized mean solution structures of Cu(I) and Cu(II) plastocyanin. The diffusion parameters for isotropic, axially symmetric, and fully anisotropic models were fit to the experimental data via minimization techniques (56). The F statistic term (57) was used to test the improvement in the statistical fit. Residues exhibiting faster internal motions or exchange broadening contributions were not included in the input file for evaluating the diffusion tensor.

The analysis of the ^{15}N relaxation rate parameters and heteronuclear NOE values was performed according to model-free formalisms by using Modelfree 4.0 program (57) within the Lipari-Szabo approach (58, 59). The S^2 values were calculated using a fixed N-H bond length of 1.02 Å and ^{15}N chemical shift anisotropy $\Delta\sigma = -172$ ppm (60). In the case of the Cu(II)-oxidized plastocyanin, the paramagnetic contribution to the experimental R_1, R_2, and NOE values was evaluated through the point-dipole approximation according to the Solomon-Bloembergen equations (61) and subtracted from the measured relaxation rates as described previously (62, 63). The longitudinal electronic relaxation rate at 14.1 tesla used in these calculations was 4×10^9 s^{-1}, as interpolated from estimates at 11.7 and 17.6 (64) as well as 18.8 tesla (65) reported for blue copper proteins.

NMR Experiments Aimed at Determining Protein Mobility in the 10^{-4}–10^{-3}-s Time Scale—The protein mobility in this time range was studied in the reduced form of the protein, at 295 K and pH 6.50. The ^{15}N nuclear spin relaxation experiments were recorded at 800.13 (^{1}H) and 81.08 MHz (^{15}N) on a Bruker Avance 800 NMR spectrometer. ^{15}N R_2 relaxation rates were measured as a function of the spin-echo delay in a series of T_2 CPMG experiments (49, 50) using different refocusing delays (τ_{CPMG} = 450, 550, 700, 850, 1000, and 1150 μs). The relaxation delay during the sequence varied from 7 to 300 ms, the exact value depending on τ_{CPMG}. The water signal was suppressed using the WATERGATE sequence (47).

NMR Experiments Aimed at Determining Protein Mobility in the 10^{-1}-1-s Time Scale—The protein mobility in this time range was indirectly studied both in reduced and oxidized forms of the protein, at 295 K and pH 6.50, through proton exchange measurements. The spectra were recorded at 800.13 (^{1}H) and 81.08 MHz (^{15}N) on a Bruker Avance 800 NMR spectrometer. Saturation transfer processes between protein amide protons and bulk water were followed by comparing the intensities of ^{1}H-^{15}N cross-peaks in two-dimensional heteronuclear single quantum coherence spectra obtained by suppressing the water signal either (i) using the WATERGATE (47) pulse sequence supplemented with a flip-back pulse (48) or (ii) using a pre-saturation pulse (900 ms) during both relaxation delay and refocusing time.

NMR Experiments Aimed at Determining Protein Mobility in the 10^2–10^5-s Time Scale—The protein mobility in this time range was studied both in both reduced and oxidized plastocyanin at 295 K and pH 6.50. Two-dimensional ^{1}H-^{15}N HSQC spectra were recorded at 800.13 (^{1}H) and 81.08 MHz (^{15}N) on a Bruker Avance 800 NMR spectrometer at different times, between 8 min and 2 days, after the addition of deuterated phosphate buffer (450 μl) to a protein solution (50 μl) in buffered H_2O. Water suppression was performed using the WATERGATE (47) pulse sequence. The intensity of the cross-peaks was fitted using a single mono-exponential decay function, yielding the rate constant for the exchange process between protein amide protons and bulk water.

RESULTS

Signal Assignment—The ^{1}H and ^{15}N NMR signals of all residues were completely or partially assigned through comparative analysis of homonuclear and heteronuclear two- and three-dimensional NMR spectra. All backbone ^{1}H and ^{15}N NMR signals were assigned, except for Ala^1, for which this was not possible because of fast exchange with the solvent. The assignment largely confirmed and further extended that reported previously(66). The full ^{1}H and ^{15}N assignment achieved in this study, together with the stereo-specific assignment, is reported in Table S1 of the Supplementary Material.

Structure Calculation—Table I reports the NMR experimental data used for the structure calculations, and Fig. 1 shows the summary of the sequential and medium range NOE connectivities involving NH, Hα, and Hβ protons.

This figure reveals the presence of several strong, short range Hα(i) − HN(i + 1) NOEs, characteristic of β-strands, that alternate with HN(i) − HN(i + 1) NOEs typical of turns. The presence of an α-helix is revealed by strong sequential HN(i) − HN(i + 1) NOEs and medium range HN(i) − HN(i + 2), Hα(i) − HN(i + 2), Hα(i) − HN(i + 3), Hα(i) − Hβ(i + 3), and Hα(i) − HN(i + 4) NOE connectivities. The presence of these secondary structure elements was supported by the restraints obtained for ϕ and ψ angles, as well as by protection of amide hydrogen atoms from exchange with solvent, as shown in Fig. 1.

Fig. 2 reports the distribution of the meaningful NOEs per residue as well as the residue-by-residue experimental constraints used for the calculation of the structure.

The 35 structures generated by TAD calculations, and having the lowest target function ($\leq$0.47 Å^2), have no consistent violations and no residual violation exceeding 0.3 Å. The global r.m.s.d. values with respect to the mean structure are 0.55 $\pm$ 0.07 and 1.14 $\pm$ 0.07 Å for the backbone and heavy atoms, respectively. The final structure-quality parameters are reported in Table I, whereas the distribution of the final backbone and heavy atoms r.m.s.d. per residue, with respect to the mean structure, is shown in Fig. 3. A "sausage" diagram of the backbone for the final DYANA family for the reduced plastocyanin from *Synechocystis* sp. PCC6803 is shown in Fig. 4*A*, and a ribbon plot for the restrained energy-minimized mean structure is shown in Fig. 4*B*.

^{15}N Relaxation Data in Cu(I) Plastocyanin—^{15}N relaxation data for reduced *Synechocystis* sp. PCC6803 plastocyanin were analyzed at 600 MHz for 91 backbone amide groups out of 94 non-proline residues. These data are shown in Fig. 5*A* and included in Table S2A of the Supplementary Material. The measured values for R_1 are within a range spanning 1.5–2.3 s^{-1}, most of them ranging from 1.8 to 2.1 s^{-1}. The values of R_2 are within the range 5.4−0.8 s^{-1}. The NOE values fall between 0.49 and the theoretical maximum of 0.834, most of them being larger than 0.73. The values for residues 17, 42, 63, and 93, which were found slightly above the theoretical maximum, were fixed to the maximum value in the Modelfree analysis.

^{15}N relaxation data for oxidized *Synechocystis* sp. PCC6803 plastocyanin were measured for 72 backbone amide groups. These data are shown in Fig. 5*B* and are included in Table S2B of the Supplementary Material. The paramagnetic contribution for the relaxation rates was higher than 0.1 s^{-1} for 12 R_1 and 13 R_2 values, for which the metal nucleus distance was shorter than 10.4 Å. The largest relative contributions of paramagnetism to R_1 correspond to residues 90 (24%), 35 (35%), and 7 (18%), whereas the paramagnetic R_2 is at most 9% of the experimental value. All data discussed below and the mobility analysis refer to R_1 and R_2 values corrected by taking into account the presence of the unpaired electron. Hereafter, the

TABLE I

Summary of NMR constraints used for DYANA structure calculation, restraint violations, structural statistics, and energetics for the restrained energy-minimized DYANA mean solution structure of reduced plastocyanin from Synechocystis sp. PCC6803

Structural constraints	Total	Violations	Root mean square violation
			Å
Meaningful (total) NOESY	1344 (1922)	22	0.014
Overall intra-residue	209		
Overall sequential	311	9	0.019
Overall medium range[a]	178	3	0.011
Overall long range	646	10	0.013
ϕ	64	1	0.111[b]
Ψ	52	2	0.154[b]
Hydrogen bonds	19	6	0.011
Copper ligand distances	4		
Overall total	1483	28	0.015
Overall violations larger than 0.3 Å			
Overall violations between 0.1 and 0.3 Å		9	
Target function (Å²)	0.38		
AMBER average total energy (kJ/mol)	−1167.5		
Structure analysis[c]			
% residues in most favored regions	81.7		
% residues in allowed regions	15.9		
% residues in generously allowed regions	2.4		
% residues in disallowed regions			
No. bad contacts/100 residues[d]			
H bond energy (kJ mol⁻¹)[d]	0.87		
Overall G-factor[d]	−0.24		

[a] Medium range distance constraints are those between residues $(i,i + 2)$ $(i,i + 3)$ $(i,i + 4)$ and $(i,i + 5)$.

[b] Degrees not included in total.

[c] According to the Ramachandran plot.

[d] The program PROCHECK was used to check the overall quality of the structure. According to the PROCHECK statistic, less than 10 bad contacts per 100 residues, an average hydrogen bond energy in the range 2.5–4.0 kJ mol⁻¹, and an overall G-factor larger than −0.5 are expected for a good quality structure (45).

experimental ^{15}N relaxation data are reported in parentheses. The values of R_1 are within a range spanning 1.25–4.25 s^{-1} (1.43–4.73 s^{-1}), with most of them ranging from 1.8 to 2.3 s^{-1} (1.8–2.5 s^{-1}); these values are similar to those observed in the reduced protein. The values of R_2 are within the range 6.6–11.1 s^{-1} (6.7–11.6 s^{-1}), with most occurring within the range between 7.5 and 9.5 s^{-1} (7.5–9.5 s^{-1}). The heteronuclear NOE values (corrected for paramagnetism) fall within 0.42 and 0.84, most of them being larger than 0.70. The values of residues 27, 32, and 57, which were found slightly above the theoretical maximum, were fixed to the maximum value in the Modelfree analysis.

On the basis of the solution NMR structures of Cu(I) and Cu(II) *Synechocystis* sp. PCC6803 plastocyanin, the three principal components of the inertia tensor are calculated to be in the ratio 1.00:0.91:0.55 and 1.00:0.92:0.55, respectively. The average values of the rotational correlation time τ_m, calculated from the R_1 and R_2 data, are 5.55 (reduced) and 5.68 ns (oxidized). These values were obtained by averaging all the τ_m values calculated from R_1 and R_2 data measured for 81 residues for the reduced protein and 63 for the oxidized form.

The results of the local diffusion analysis of the ^{15}N relaxation data in both oxidation states indicate that the relaxation is best described using an axially symmetric diffusion tensor. This model for the overall tumbling of plastocyanin provided a statistically significant improvement over the isotropic model, yielding an F statistic value of 4.7 for Cu(II) plastocyanin and of 5.6 for the Cu(I) form. The use of a fully anisotropic model does not give a statistically significant improvement compared with the axially symmetric model for either oxidation state (F = 0.3–0.7). The final optimization of the axially symmetric model results in values of τ_m = 5.75 ± 0.05 ns (reduced) and 5.87 ± 0.05 ns (oxidized).

Model-free Analysis—The analysis of the ^{15}N relaxation rate parameters and heteronuclear NOE values was performed ac-
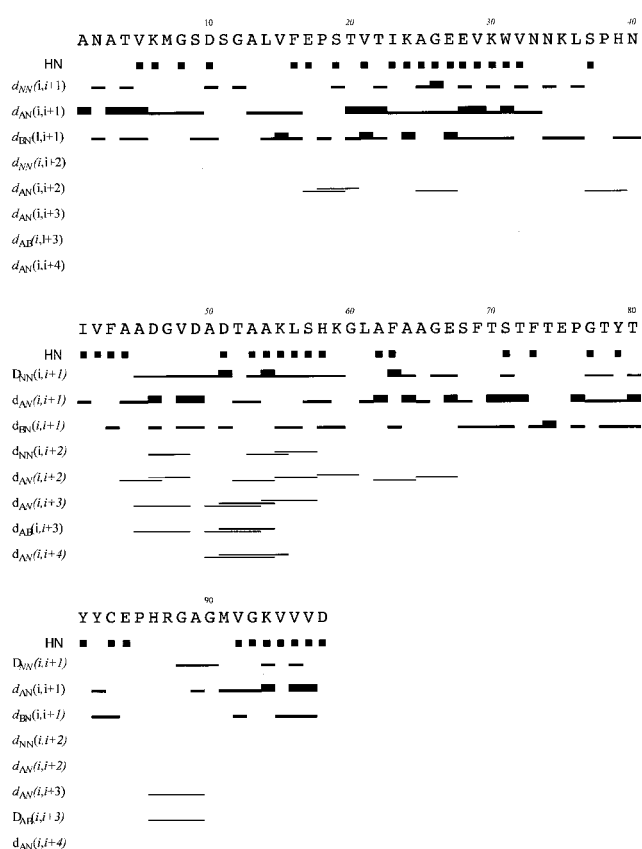

FIG. 1. **Schematic plot of sequential and medium range NOEs involving NH, Hα, and Hβ protons in reduced *Synechocystis* sp. PCC6803 plastocyanin.** The *thickness* of the *bar* represents the intensity of the NOESY cross-peaks. The slowly exchanged NH protons used for structural constraints are indicated in the *upper panel*.
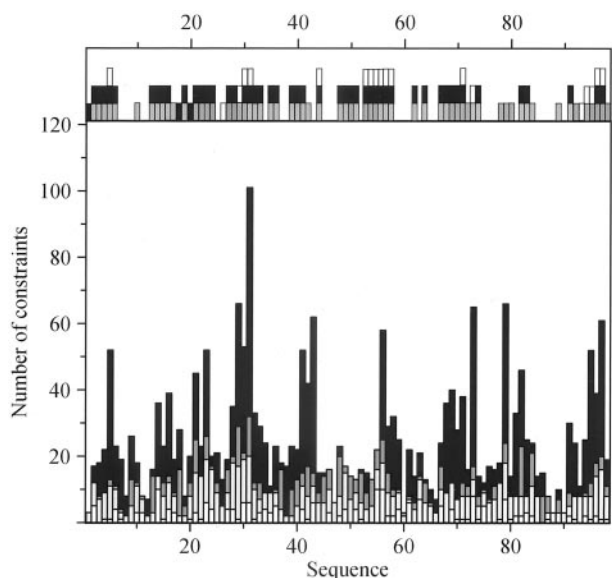
FIG. 2. **Distribution of meaningful NOEs per residue, used for structure calculation of reduced *Synechocystis* PCC6803 plastocyanin.** Intra-residue, sequential, medium range, and long range NOE constraints are in *white, light gray, dark gray,* and *black,* respectively. In the *top panel* the residue-by-residue constraints, other than NOEs, used for the calculation (hydrogen bonds, *white bars*; ϕ dihedral angle constraints, *gray bars*, ψ dihedral angles, *black bars*) are also reported.
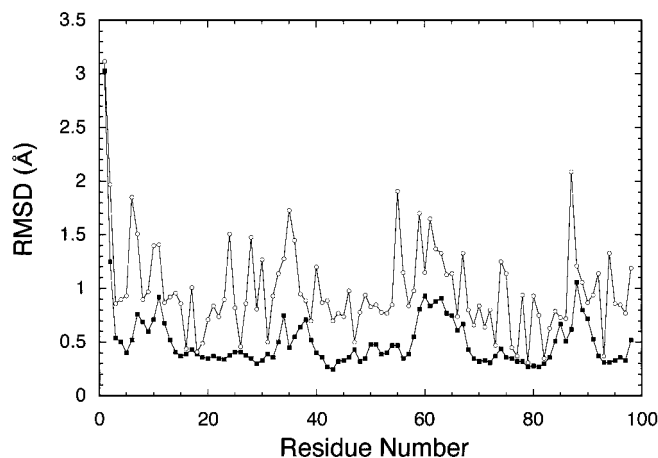

FIG. 3. **Diagram of global backbone (■) and heavy atoms (○) r.m.s.d. per residue with respect to the mean structure for the 35 DYANA structures of reduced *Synechocystis* sp.** PCC6803 plastocyanin.

FIG. 4. *A,* sausage diagram of the superimposed 35 DYANA backbone structures of reduced *Synechocystis* sp. PCC6803 plastocyanin. *B,* ribbon drawing of the restrained, energy-minimized DYANA mean structure of reduced *Synechocystis* sp. PCC6803 plastocyanin showing the elements of secondary structure in different colors. *C,* comparison of the energy-minimized mean DYANA solution structures of reduced (*orange*) and oxidized (*purple*) plastocyanin.

cording to the model-free formalism by using the Modelfree 4.0 program (57) within the Lipari-Szabo approach (58, 59). In the case of an axially symmetric diffusion tensor, the general expression for $J(\omega)$ is shown in Equation 1,

$$J(\omega) = \frac{2}{5}S_f^2 \sum_{i=1}^{3} A_j \left[\frac{S_s^2 \tau_j}{1 + (\omega\tau_j)^2} + \frac{(1 - S_s^2)\tau_j'}{1 + (\omega\tau_j')^2} \right] \quad \text{(Eq. 1)}$$

where S_f^2 and S_s^2 are the squares of the order parameters characterizing the amplitude of the internal motions for the fast (<20 ps) and slow (>20 ps) time scales, respectively; $\tau_j' = \tau_j \tau_e/(\tau_{j + e})$, $\tau_1^{-1} = 6D_\perp$, $\tau_2^{-1} = 5D_\perp + D_\parallel$, $\tau_3^{-1} = 2D_\perp + 4D_\parallel$, τ_e is the effective correlation time for the slow (>20 ps) internal motions, $A_1 = (3\cos^2\vartheta - 1)^2/4$, $A_2 = 3\cos^2\vartheta\sin^2 74$, $A_3 = (3/4)\sin^4\vartheta$, and ϑ is the angle between the N-H bond vector and the unique axis of the principal frame of the diffusion tensor, D. $S^2 = S_f^2 S_s^2$ is the square of the generalized order parameter for
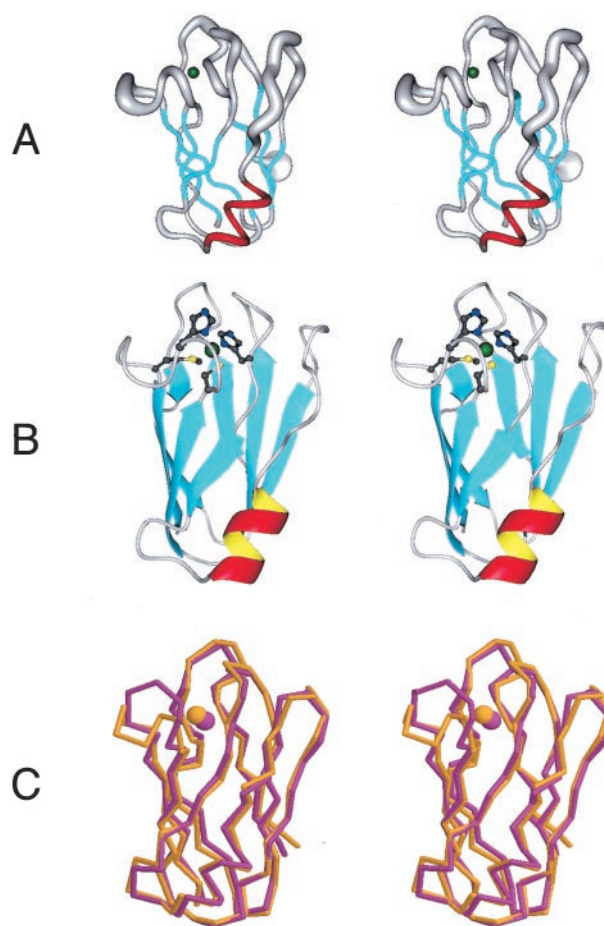
internal motion. In order to take into account the presence of a contribution to the experimental ^{15}N R_2 relaxation rate from conformational exchange processes, an additional adjustable parameter (R_{ex}), which sums up to the value of R_2 calculated taking into account only the dipolar and chemical shift anisotropy contributions, may be introduced. In the approach implemented in the Modelfree program, one can assume different models for internal motions, which correspond to assuming different forms for the spectral density function $J(\omega)$. Given the availability of three relaxation parameters (^{15}N R_1, ^{15}N R_2, ^{15}N-^{1}H NOE) measured at a single static magnetic field, no more than three model-free parameters can be fit to these data. Therefore, the data were treated according to either model 1 ($S_f^2 = 1$, $\tau_e \ll \tau_j$, $R_{ex} = 0$, the only parameter being S_s^2), model 2 ($S_f^2 = 1$, $R_{ex} = 0$, the parameters being S_s^2 and τ_e), model 3 ($S_f^2 = 1$, $\tau_e \ll \tau_j$, the parameters being S_s^2 and R_{ex}), model 4 ($S_f^2 = 1$, the parameters being S_s^2, τ_e, and R_{ex}), and model 5 ($R_{ex} = 0$, the parameters being S_s^2, S_f^2, and τ_e). Model selection for the Modelfree calculations was performed according to the procedure described previously (57).

Relaxation data from 91% (reduced) and 93% (oxidized) of the residues considered for analysis could be satisfactorily fit using model 1. The relaxation data of Lys[35], Asp[46], Gly[47], Val[48], and Asp[49] could be accounted for by using model 2 in both redox forms. Residues His[39], Gly[88], and Met[91] were best fit by assuming a modest R_{ex} contribution (model 3) in the reduced form,
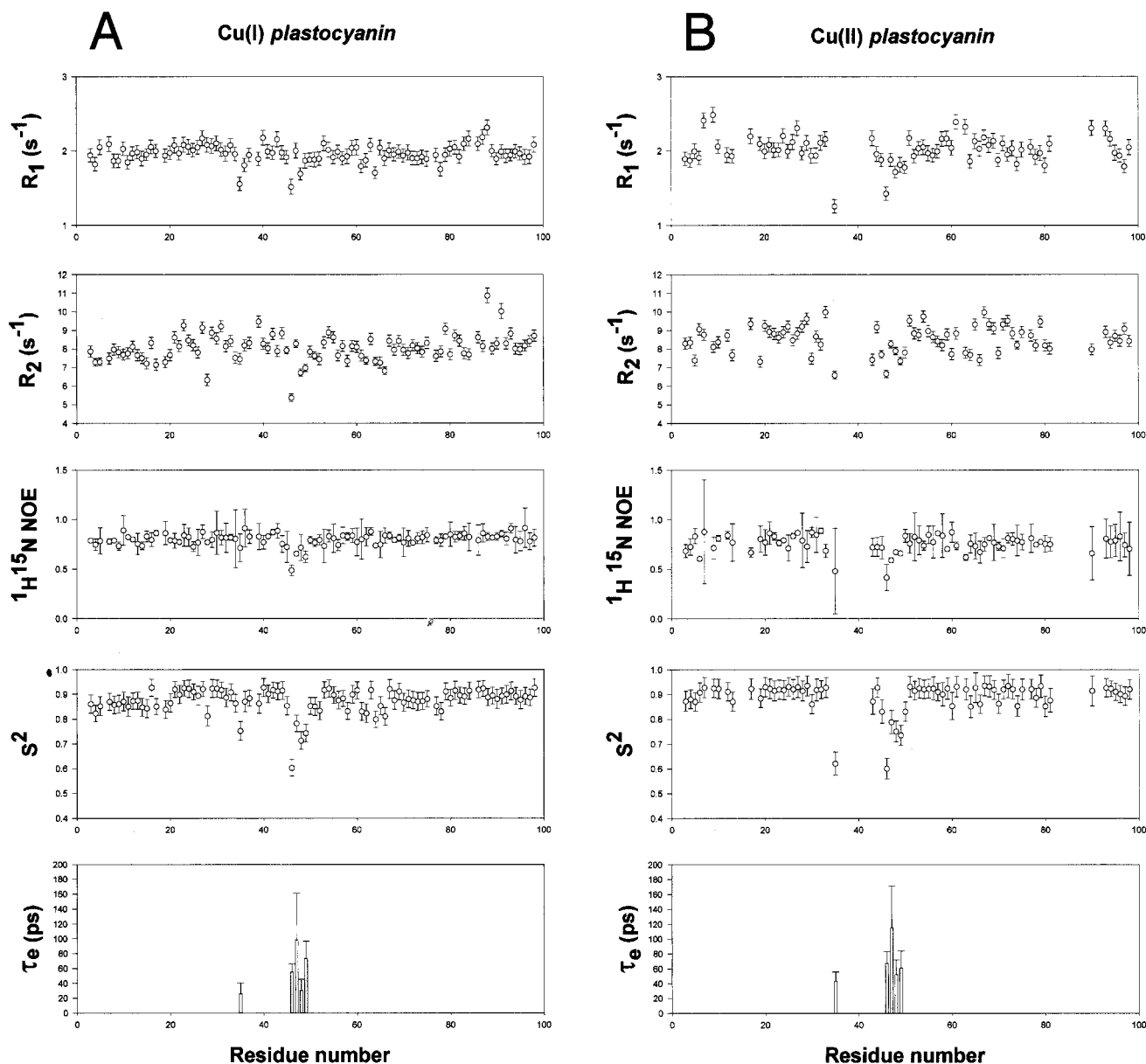
FIG. 5. **Experimental ^{15}N relaxation data and calculated S^2 and τ_e parameters for reduced (*A*) and oxidized (*B*) *Synechocystis* sp. PCC6803 plastocyanin.**

whereas their corresponding cross-peaks were not observed in the oxidized form.

In the case of the oxidized protein, residues Leu[14] and Leu[36] could not be fit to any of the models 1–3. Fits using either model 4 or model 5 gave no statistically significant improvement. Residues 14 and 36 are located in two loops of the northern region of the protein, near the copper ion. The protein structure in this region is characterized by high r.m.s.d. values (29), and for this reason the uncertainty in the metal-nucleus distance can lead to significant errors in the estimation of the paramagnetic contribution. Another explanation for failure to fit the relaxation data for these residues to any of the models is the observed low intensity of their ^{1}H-^{15}N cross-peaks, due to line broadening caused, in turn, by the vicinity of the paramagnetic copper ion. These residues were discarded from the final model-free analysis.

The order parameters S^2 for both redox forms of the plastocyanin are reported in Fig. 5. Average S^2 values calculated over all residues were 0.87 ± 0.05 (reduced) and 0.89 ± 0.06 (oxidized). Residues involved in regular secondary structure ele-

ments are characterized by average S^2 values of 0.88 (β-sheets) and 0.87 (α-helix) in the reduced protein and 0.91 (β-sheets) and 0.90 (α-helix) in the oxidized form. Residues located in non-structured regions display average S^2 values of 0.86 (reduced) and 0.85 (oxidized).

The residues for which the additional τ_e parameter (model 2) was needed to fit the relaxation data (35, 46–49) featured values for τ_e in the range of 20–100 (reduced) and 40–120 ps (oxidized). The residues described by model 3 in the reduced protein (39, 88, and 91) required values for R_{ex} smaller than 2 Hz for the fitting procedure.

Analysis of Protein Mobility in the Longer Time Scales—The Modelfree analysis has shown that no residue is affected by a substantial R_{ex} contribution in any of the two redox forms. A CPMG experiment at 800 MHz with variable delays in the reduced protein has confirmed that no exchange is detected in the range 0.45–1.15 ms. This result has discouraged us from extending the measurements to the oxidized form or to shorter time scales through $T_{1\rho}$ measurements.

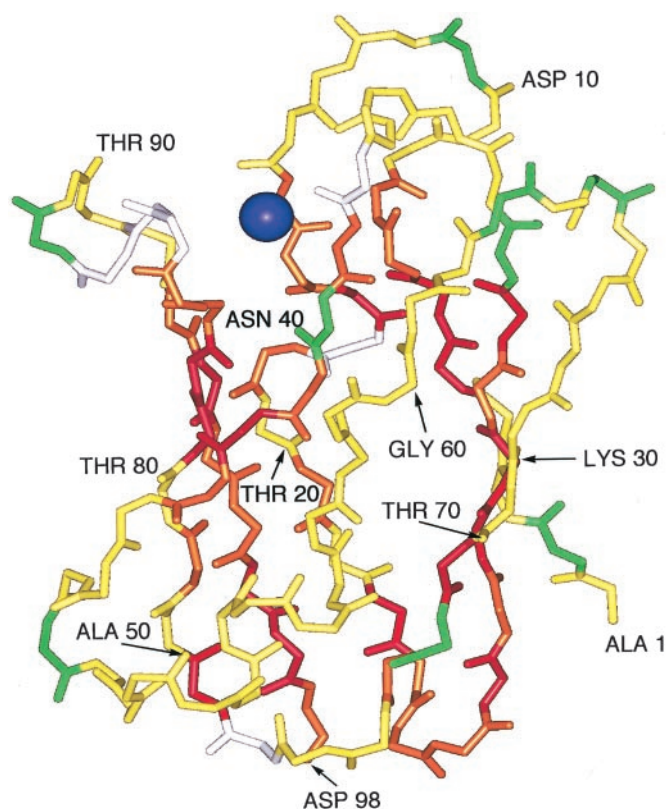Investigation of the protein mobility in the time range

FIG. 6. **Backbone of energy-minimized mean DYANA solution structure of reduced *Synechocystis* sp.** PCC6803 plastocyanin color coded according to the peptide amide protons exchange rate R_{exch} (*red*, $R_{exch} \leq 10^{-6}$ s^{-1}; *orange*, $10^{-6} < R_{exch} < 10^{-3}$ s^{-1}; *yellow*, $10^{-3} < R_{exch} < 1$ s^{-1}; *green*, $R_{exch} > 1$ s^{-1}). Relevant hydrogen bonds are displayed.

10^{-1}–1 s was carried out indirectly. The intensities of amide ^{1}H-^{15}N cross-peaks in two-dimensional HSQC spectra were measured by suppressing the water signal either by using the WATERGATE/flip-back pulse sequence or by using a low power 900-ms pre-saturation pulse during both relaxation delay and refocusing time. A number of NH cross-peaks were characterized by a significant decrease ($\geq 60\%$) of the cross-peak intensity in the spectrum obtained upon solvent suppression using the pre-saturation pulse. None of these NH protons is closer than 2.4 Å to a CHα proton that lies within 0.2 ppm from the saturated water peak, so that NOE contributions to the observed effect should be smaller than 10% (67). This large decrease indicates that the corresponding amide NH protons experience exchange processes with the bulk solvent during the pre-saturation time. The nine amino acids that were identified in this manner (residues 2, 11, 33, 40, 47, 63, 65, 72, and 88 in Fig. 6) are conserved in both reduced and oxidized plastocyanin and are characterized by the absence of a hydrogen bond network for the NH proton.

The protein mobility in the longer time range (10^2–10^5 s) was investigated by estimating the rate constant (R_{exch}) for the hydrogen/deuterium exchange of amide NH groups in the reduced and oxidized forms of the protein. In both cases the amide protons were divided into three classes: (i) intermediate exchange ($10^{-6} < R_{exch} < 10^{-3}$ s^{-1}, can be estimated by a fit of the intensity *versus* time), (ii) fast exchange ($R_{exch} > 10^{-3}$ s^{-1}, not obtained by a fit because the intensity decreases drastically before the end of data collection for the first spectrum), and (iii) slow exchange ($R < 10^{-6}$ s^{-1}, not obtained by the fit because the intensity remains essentially constant throughout the experiment). The residues belonging to these three classes, together with those exchanging in the 10^{-1}–1 s time scale, are

color-coded and are shown in Fig. 6. Overall, the results indicate that most amide protons for reduced plastocyanin are in exchange with the solvent. No significant differences are observed concerning the distribution of the residues in the three above classes between the reduced and oxidized forms. Within the intermediate exchange class, where more subtle differences can be appreciated, the exchange rate constant is the same within the statistical error for most residues. In the very few cases where a small statistical difference is determined, the rate constant for the reduced form is 2–4 times higher than in the oxidized form.

DISCUSSION

An Analysis of the Structure of the Reduced Protein—The structure family has a low r.m.s.d. across the sequence, with the lowest r.m.s.d. found in the regions containing regular secondary structure (Fig. 3). The backbone pairwise r.m.s.d. between such regions is 0.68 $\pm$ 0.11 Å, whereas that calculated over all residues is 0.79 $\pm$ 0.11 Å. Table II reports the r.m.s.d. determined by separately superimposing the secondary structure elements of the final ensemble of 35 DYANA structures.

Fig. 3 and Table II reveal that significantly higher r.m.s.d. values are found in the loops as compared with the regions possessing regular secondary structure. In particular, there are four regions in the structure that feature high r.m.s.d. values as follows: Gly[8]–Val[15], Asn[34]–Ile[41], His[58]–Glu[67], and Pro[85]–Met[91]. These regions are clearly revealed by the "sausage" diagram of the backbone for the final DYANA family as shown in Fig. 4*A*, which also indicates their length and proximity to the copper ion. Altogether, these four disordered regions define the hydrophobic patch in the northern part of the protein surface surrounding the copper site. This apparent disorder can be ascribed to the lower-than-average number of NOEs per residue observed for this region (see Fig. 2), even though all observed ^{1}H NOESY cross-peaks for the residues included in these regions have been assigned and used for structure calculation. Additionally, the first, second, and fourth regions each contain two glycine residues (Gly[8]/Gly[12], Gly[60]/Gly[66], and Gly[88]/Gly[90]) which usually give few dipolar constraints as a consequence of their intrinsically small number of protons.

A ribbon plot for the restrained energy-minimized DYANA family mean structure of the reduced plastocyanin from *Synechocystis* sp. PCC6803 is shown in Fig. 4*B*. In comparison with other plastocyanins, the solution structure of this protein is characterized by the presence of a fold made of extended β-sheets that are connected by inter-strand loops and a short α-helix. In particular, the protein is composed of eight β-strands organized in two twisted sheets. The first β-sheet is composed of four strands formed by residues Ala[3]–Met[7] (strand S1), Phe[16]–Glu[17] (strand S2A), Glu[27]–Asn[33] (strand S3), and Ser[68]–Phe[73] (strand S6). The β-strands involving residues Thr[20]–Ile[23] (strand S2B), Val[42]–Ala[44] (strand S4), His[58]–Ala[62] (strand S5, β-bulge), Gly[77]–Tyr[82] (strand S7), and Val[92]–Val[97] (strand S8) constitute the second β-sheet. Both β-sheets have mixed parallel and anti-parallel strands connected by several turns and loops. The protein has a α-helix that consists of seven residues (Ala[50]–Leu[56]) and contains two complete helical turns. The protein does not have any other regular secondary structure in addition to the above-mentioned structural motifs.

Comparison between the Solution Structures of Reduced and Oxidized Plastocyanin—The elements of secondary structure correspond well to those found for the oxidized form of the plastocyanin from *Synechocystis* sp. PCC6803 (29) and are similar to those of other plastocyanins (Fig. 4*C*). Table II

TABLE II

Structural statistics for the ensemble of 35 DYANA structures of reduced plastocyanin from Synechocystis sp. PCC6803 and comparison with the oxidized form

This table reports the global pairwise r.m.s.d. for backbone (BB) and heavy atoms (HA) obtained by superimposing the specified selected fragments.

Structural motif	BB-reduced	HA-reduced	BB-oxidized[a]	BB-oxidized *versus* reduced
		Å		
Backbone[b]	0.79 ± 0.11	1.63 ± 0.11	1.03 ± 0.18	1.21
Secondary structure[c]	0.68 ± 0.11	1.57 ± 0.13	0.64 ± 0.11	0.68
Sheet I[d]	0.49 ± 0.10	1.47 ± 0.17	0.47 ± 0.09	0.49
Sheet II[e]	0.65 ± 0.13	1.48 ± 0.16	0.68 ± 0.15	0.64
Helix[f]	0.25 ± 0.08	1.53 ± 0.30	0.20 ± 0.06	0.14
All loops[g]	0.83 ± 0.13	1.64 ± 0.16	1.29 ± 0.27	1.58
Copper-binding loops[h]	0.70 ± 0.17	1.69 ± 0.24	1.44 ± 0.39	1.79
Non-Copper-binding loops[i]	0.72 ± 0.14	1.44 ± 0.16	0.92 ± 0.23	0.85

[a] From Ref. 29.
[b] Residues 3–96.
[c] Sheet I, sheet II, and helix.
[d] Residues 3–7, 16–17, 27–33, and 68–73.
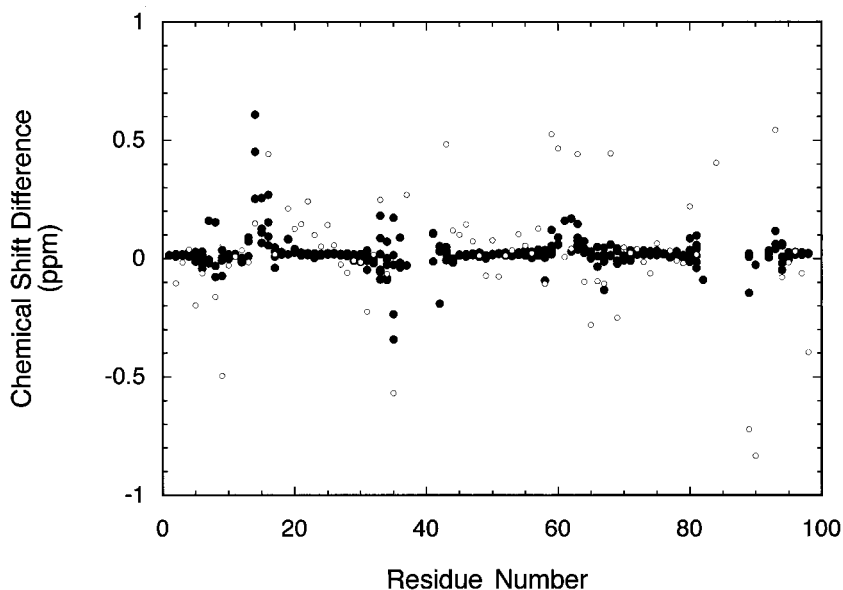[e] Residues 20–23, 42–44, 58–62, 77–82, and 92–97.
[f] Residues 50–56.
[g] Residues 8–15, 18–19, 24–26, 34–41, 45–49, 57, 63–67, 74–76, and 83–91.
[h] Residues 34–41 and 83–91.
[i] Residues 8–15, 18–19, 24–26, 45–49, 57, 65–67, and 74–76.

FIG. 7. **Differences in ^{1}H (●) and ^{15}N (○) chemical shifts between oxidized and reduced forms of *Synechocystis* sp. PCC6803 plastocyanin.**

shows that the distribution of the r.m.s.d. for the DYANA families is similar for both structures and reveals the greatest uncertainties in the northern-face loop regions mentioned above. This observation indicates that the paramagnetism of the Cu(II) ion in the oxidized form of the protein is not the only physical phenomenon hindering the determination of the structure in these loops (see below), because the same uncertainties are maintained in the diamagnetic, reduced Cu(I) form of the protein. The overall global backbone r.m.s.d. between the energy-minimized, mean DYANA solution structures of reduced and oxidized plastocyanin is 1.21 Å (see Table II). This is mostly due to displacements of entire secondary structure elements, in turn arising from the lower structural resolution of the loops connecting them.

Even though the above-described analysis indicates the absence of significant structural differences between the two redox forms of plastocyanin, small differences may still be present. In particular, differences in the metal-binding site would be the most interesting to monitor. To address this point further, an analysis of the ^{1}H and ^{15}N chemical shift differences between the reduced and oxidized forms of plastocyanin was performed.[2] These differences are expected to be very sensitive to small structural modifications. Fig. 7 shows that ^{1}H and ^{15}N chemical shift differences are found in the regions encompassing all four northern loops, whereas none of the regions around the southern loops are involved. Whereas ^{15}N chemical shift differences have been discussed in terms of very minor steric/electronic variations (69–75), the ^{1}H chemical shift differences can be tentatively ascribed to modest structural modifications consequent to a redox state change of the copper ion, as also found in a similar analysis for pea plastocyanin (72).

Backbone Mobility in Reduced and Oxidized Plastocyanin— Recently, ^{15}N relaxation measurements of two blue copper proteins in their reduced form, namely *Pseudomonas aeruginosa* azurin (30) and *P. pantotrophus* pseudoazurin (31), have indicated that proteins of this class are rigid (the average S^2 values for these proteins were 0.86 and 0.83, respectively). In the present investigation we extended this picture to the dy-

---

[2] The chemical shifts of the oxidized form were corrected to account for pseudocontact contribution, whereas the contact shift contribution is limited to the copper-coordinated residues (68).

namic behavior of a reduced plastocyanin as well as to its oxidized state.

The backbone relaxation data on *Synechocystis* sp. PCC6803 plastocyanin, and the subsequent model-free analysis, show that this protein is a rigid molecule in both redox forms. The protein exhibits no significant backbone motions in the picosecond to nanosecond time scale (Fig. 5). This behavior parallels the results obtained on azurin and pseudoazurin and is not unexpected for a protein with a high β-sheet content. Recent mutagenesis studies have revealed that enhanced mobility in one of the loops of azurin does not alter the overall rigidity of the molecule (76). In addition, the β-barrel scaffold found in amicyanin is able to accommodate different engineered loops while maintaining the particular electronic features of the blue copper site (77). In general, the presence of a high loop content around the copper site in cupredoxins may provide a compromise solution regarding mobility. The structure is rigid enough to allow the protein to accommodate different redox states but at the same time provides a relatively flexible interface for protein-protein recognition in electron transfer processes.

The mobility features of *Synechocystis* sp. PCC6803 plastocyanin in the sub-nanosecond range along the protein sequence are very similar in the two redox states (Fig. 5). The residues 46–49, located in a loop between β-strand S4 and the α-helix, show higher than average mobility. Attempts to crystallize this protein in its native form were unsuccessful, whereas crystallization of a triple mutant (Ala[44] → Asp/Asp[49] → Pro/Ala[65] → Leu) resulted in the determination of its x-ray structure (13). These mutations do not alter the overall protein fold as found by comparison with the solution structure of the protein in both forms (this work and Ref. 29). However, two of these mutations occur in the vicinity of the mobile region described above, suggesting that a mobility decrease, due to the introduced mutations, could contribute to crystal stabilization.

Three residues (His[39], Gly[88], and Met[91]) required a modest chemical exchange contribution to R_2 in the reduced protein. These residues are located in the northern loops of the molecule, and this observed mobility may contribute to the lower structural resolution observed by NMR in these regions. In the oxidized protein, the paramagnetism of the nearby Cu(II) ion prevented observation of the heteronuclear cross-peak for these amino acids, and a comparison with the reduced form cannot be accomplished.

The two redox forms are also similar on the longer time scales investigated in the present work. No significant differences were detected in the exchange of amide NH groups with water. In this time frame, only backbone amide protons not involved in hydrogen bonds are found to exchange with bulk water (Fig. 6). Overall, only 16 out of 94 non-proline HSQC cross-peaks display unaltered intensity after 2 days of contact with a large excess of D_2O, indicating that their corresponding protons are not exchangeable. This is consistent with the presence of strong hydrogen bonds involving these protons, located in the core regions of β-sheets, and with their solvent inaccessibility as calculated using the WHATIF program (78). Some of the exchanging protons (17 in total) are inaccessible to solvent and therefore must undergo conformational changes in order to interact with bulk water. These latter residues are mainly located in the northern loops comprising residues Gly[8]–Val[15] and Asn[34]–Ile[41]. The two remaining northern loops are characterized by both solvent exchange phenomena and by a significant solvent accessibility, the latter precluding a definitive conclusion about their mobility in the longer time scales. The relatively large r.m.s.d. for the structure family in these loop regions can therefore, at least for the first two loops, be as-

cribed to protein mobility. Presumably, the same holds also for the C terminus loops.

The observed independence of protein dynamics from the copper ion oxidation state somewhat contrasts analogous data obtained for other redox metalloproteins. For example, *c*-type cytochromes experience much larger H/D exchange rates in the oxidized form rather than in the reduced form (79–88) which is paralleled by higher values of $R_{1\rho}$ (89). [15]N relaxation data (90), $R_{1\rho}$ experiments (91), as well as H/D exchange phenomena (92) reveal an increased mobility in the oxidized form also in the case of cytochrome b_5. In the case of putidaredoxin, a [Fe$_2$S$_2$] protein, the oxidized form again exhibits higher mobility than the reduced species in the sub-nanosecond and micro-millisecond time scale (93), and this behavior is paralleled by H/D exchange measurements (94). It would appear as if the present cupredoxin, representative of the third large class of electron transfer proteins, constitutes an exception. However, recent studies on cytochrome b_{562} show that there are no significant differences in NH mobility in the subnano- and microsecond time scales for the two oxidation states.[3] Apparently, the determinants for the differences in mobility of electron transfer proteins in the two oxidation states are complex and not immediately rationalized. It could be speculated that both cytochrome b_{562} (a four-helix bundle) and blue copper proteins (all-β-fold) have extended elements of secondary structure and a well defined hydrophobic core. This is somewhat less true of putidaredoxin and even less true for cytochromes, which could make the mobility of the latter proteins more sensitive to a change in the charge of the metal center.

Concluding Remarks—Mobility studies have been performed on the reduced plastocyanin from *Synechocystis* sp. PCC6803 and, for the first time, also on the oxidized protein under the same experimental conditions on a broad time scale range (from $\sim 10^{-11}$ to 10^5 s). This analysis has revealed that plastocyanin is a rigid molecule in both redox states, in the sub-millisecond time scale. On the other hand, mobility studies in the milliseconds and longer time scales show significant protein flexibility in both redox states, localized on the northern loops near the copper ion. This finding might have significant impact for the physiological redox transfer role of plastocyanins. The solution structure of the reduced plastocyanin from *Synechocystis* sp. PCC6803 is also reported to a good quality of resolution. Despite the close similarity between the structure of reduced and oxidized plastocyanin, ^{1}H and ^{15}N chemical shift differences suggest that small structural rearrangements, localized in the same northern loops, may occur upon the redox change. In conclusion, the complementary applications of structure and dynamic studies have provided a full characterization of these systems in solution.

REFERENCES

1. Redinbo, M. R., Yeates, T. O., and Merchant, S. (1994) *J. Bioenerg. Biomembr.* **26,** 49–66
2. Navarro, J. A., Hervàs, M., and De la Rosa, M. A. (1997) *J. Biol. Inorg. Chem.* **2,** 11–22
3. Sigfridsson, K. (1998) *Photosynth. Res.* **57,** 1–28
4. Hope, A. B. (2000) *Biochim. Biophys. Acta* **1456,** 5–26
5. Adman, E. T. (1991) *Adv. Protein Chem.* **42,** 144–197
6. Sykes, A. G. (1991) *Struct. Bonding* **75,** 175–224
7. Malmstrom, B. G. (1994) *Eur. J. Biochem.* **223,** 711–718
8. Gray, H. B., Malmstrom, B. G., and Williams, R. J. P. (2000) *J. Biol. Inorg. Chem.* **5,** 551–559
9. Sandman, G. (1986) *Arch. Microbiol.* **145,** 76–79
10. Bryant, D. A. (1994) *The Molecular Biology of Cyanobacteria*, Kluwer Aca-

[3] M. Assfalg, L. Banci, P. D. Barker, I. Bertini, and S. Ciofi, submitted for publication.

demic Publishers Group, Dordrecht, Netherlands

11. Guss, J. M., and Freeman, H. C. (1983) *J. Mol. Biol.* **169,** 521–563
12. Badsberg, U., Jorgensen, A. M. M., Gesmar, H., Led, J. J., Hammerstad, J. M., Jespersen, L. L., and Ulstrup, J. (1996) *Biochemistry* **35,** 7021–7031
13. Romero, A., De la Cerda, B., Vareda, P. F., Navarro, J. A., Hervas, M., and De la Rosa, M. A. (1998) *J. Mol. Biol.* **275,** 327–336
14. Ma, L., Jorgensen, A.-M. M., Sorensen, G. O., Ulstrup, J., and Led, J. J. (2000) *J. Am. Chem. Soc.* **122,** 9473–9485
15. Sun, J., Xu, W., Hervas, M., Navarro, J. A., De la Rosa, M. A., and Chitnis, P. R. (1999) *J. Biol. Chem.* **274,** 19048–19054
16. Guss, J. M., Harrowell, P. R., Murata, M., Norris, V. A., and Freeman, H. C. (1986) *J. Mol. Biol.* **192,** 361–387
17. Guss, J. M., Bartunik, H. D., and H. C., F. (1992) *Acta Crystallogr. Sect. B Struct. Sci.* **48,** 790–811
18. Collyer, C. A., Guss, J. M., Sugimura, Y., Yoshizaki, F., and Freeman, H. C. (1990) *J. Mol. Biol.* **211,** 617–632
19. Redinbo, M. R., Cascio, D., Choukair, M. K., Rice, D., Merchant, S., and Yeates, T. O. (1993) *Biochemistry* **32,** 10560–10567
20. Shibata, N., Inoue, T., Nagano, C., Nishio, N., Kohzuma, T., Onodera, K., Yoshizaki, F., Sugimura, Y., and Kai, Y. (1999) *J. Biol. Chem.* **274,** 4225–4230
21. Xue, Y., Okvist, M., Hansson, O., and Young, S. (1998) *Protein Sci.* **7,** 2099–2105
22. Bond, C. S., Bendall, D. S., Freeman, H. C., Guss, J. M., Howe, C. J., Wagner, M. J., and Wilce, M. C. (1999) *Acta Crystallogr. Sect. D Biol. Crystallogr.* **55,** 414–421
23. Inoue, T., Gotowda, M., Sugawara, H., Kohzuma, T., Yoshizaki, F., Sugimura, Y., and Kai, Y. (1999) *Biochemistry* **38,** 13853–13861
24. Inoue, T., Sugawara, H., Hamanaka, S., Tsukui, H., Suzuki, E., Kohzuma, T., and Kai, Y. (1999) *Biochemistry* **38,** 6063–6069
25. Sugawara, H., Inoue, T., Li, C., Gotowda, M., Hibino, T., Takabe, T., and Kai, Y. (1999) *J. Biochem. (Tokyo)* **125,** 899–903
26. Babu, C. R., Volkman, B. F., and Bullerjahn, G. S. (1999) *Biochemistry* **38,** 4988–4995
27. Moore, J. M., Lepre, C. A., Gippert, J. P., Chazin, W. J., Case, D. A., and Wright, P. E. (1991) *J. Mol. Biol.* **221,** 533–555
28. Bagby, S., Driscoll, P. C., Harvey, T. S., and Hill, H. A. O. (1994) *Biochemistry* **33,** 6611–6622
29. Bertini, I., Ciurli, S., Dikiy, A., Fernandez, C., Luchinat, C., Safarov, N., Shumilin, S., and Vila, A. (2001) *J. Am. Chem. Soc.* **123,** 2405–2413
30. Kalverda, A. P., Ubbink, M., Gilardi, G., Wijmenga, S. S., Crawford, A., Jeuken, L. J. C., and Canters, G. W. (1999) *Biochemistry* **38,** 12690–12697
31. Thompson, G. S., Leung, Y.-C., Ferguson, S. J., Radford, S. E., and Redfield, C. (2000) *Protein Sci.* **9,** 846–858
32. Hervas, M., Navarro, F., Navarro, J. A., Chavez, S., Diaz, A., Florencio, F. J., and De la Rosa, M. A. (1993) *FEBS Lett.* **319,** 257–260
33. Studier, F. W., Rosenberg, A. H., Dunn, J. J., and Dubendorff, J. W. (1990) *Methods Enzymol.* **185,** 66–89
34. Kato, S., Shiratori, I., and Takamiya, A. (1962) *J. Biochem. (Tokyo)* **51,** 32–40
35. Bradford, M. M. (1976) *Anal. Biochem.* **72,** 248–254
36. Bartels, C., Xia, T., Billeter, M., Guntert, P., and Wuthrich, K. (1995) *J. Biomol. NMR* **6,** 1–10
37. Wuthrich, K. (1986) *NMR of Proteins and Nucleic Acids*, John Wiley & Sons, Inc., New York
38. Arseniev, A., Schultze, P., Worgotter, E., Braun, W., Wagner, G., Vasak, M., Kagi, J. H., and Wuthrich, K. (1988) *J. Mol. Biol.* **201,** 637–657
39. Vuister, G. W., and Bax, A. (1993) *J. Am. Chem. Soc.* **115,** 7772–7777
40. Guntert, P., Mumenthaler, C., and Wuthrich, K. (1997) *J. Mol. Biol.* **273,** 283–298
41. Gagné, S. M., Tsuda, S., Lee, M. X., Chandra, M., Smillie, L. B., and Sykes, B. D. (1994) *Protein Sci.* **3,** 1961–1974
42. Guntert, P., Braun, W., and Wuthrich, K. (1991) *J. Mol. Biol.* **217,** 517–530
43. Koradi, R., Billeter, M., and Wuthrich, K. (1996) *J. Mol. Graphics* **14,** 51–55
44. Pearlman, D. A., Case, D. A., Caldwell, J. W., Ross, W. S., Cheatham, T. E., Ferguson, D. M., Seibel, G. L., Singh, U. C., Weiner, P. K., and Kollman, P. A. (1997) Amber 5.0, University of California, San Francisco
45. Laskowski, R. A., MacArthur, M. W., Moss, D. S., and Thornton, J. M. (1993) *J. Appl. Crystallogr.* **26,** 283–291
46. Marion, D., and Wuthrich, K. (1983) *Biochem. Biophys. Res. Commun.* **113,** 967–974
47. Sklenar, V., Piotto, M., Leppik, R., and Saudek, V. (1993) *J. Magn. Reson.* **102,** 241–245
48. Grzesiek, S., and Bax, A. (1993) *J. Am. Chem. Soc.* **115,** 12593–12594
49. Peng, J. W., and Wagner, G. (1994) *Methods Enzymol.* **239,** 563–595
50. Kay, L. E., Nicholson, L. K., Delaglio, F., Bax, A., and Torchia, D. A. (1992) *J. Magn. Reson.* **97,** 359–375
51. Marquardt, D. W. (1963) *J. Soc. Ind. Appl. Math.* **11,** 431–441
52. Press, W. H., Flannery, B. P., Teukolsky, S. A., and Vetterling, W. T. (1988) *Numerical Recipes in C: The Art of Scientific Computing*, Cambridge University Press, New York
53. Zinn-Justin, S., Berthault, P., Guenneugues, M., and Desvaux, H. (1997) *J. Biomol. NMR* **10,** 363–372
54. Palmer, A. G. I., Rance, M., and Wright, P. E. (1991) *J. Am. Chem. Soc.* **113,** 4371–4380
55. Peng, J. W., and Wagner, G. (1992) *Biochemistry* **31,** 8571–8586
56. Lee, L. K., Rance, M., Chazin, W. J., and Palmer, A. G. I. (1997) *J. Biomol. NMR* **9,** 287–298
57. Mandel, M. A., Akke, M., and Palmer, A. G. I. (1995) *J. Mol. Biol.* **246,** 144–163
58. Lipari, G., and Szabo, A. (1982) *J. Am. Chem. Soc.* **104,** 4546–4559
59. Lipari, G., and Szabo, A. (1982) *J. Am. Chem. Soc.* **104,** 4559–4570
60. Ishima, R., and Torchia, D. A. (2000) *Nat. Struct. Biol.* **7,** 740–743
61. Solomon, I. (1955) *Phys. Rev.* **99,** 559–565
62. Arnesano, F., Banci, L., Bertini, I., Koulougliotis, D., and Monti, A. (2000) *Biochemistry* **39,** 7117–7130
63. Bertini, I., Luchinat, C., and Niikura, Y. (2000) *Proteins Struct. Funct. Genet.* **41,** 75–85
64. Ma, L., and Led, J. J. (2000) *J. Am. Chem. Soc.* **122,** 7823–7824
65. Bertini, I., Fernandez, C. O., Karlsson, B. G., Leckner, J., Luchinat, C., Malmstrom, B. G., Nersissian, A. M., Pierattelli, R., Shipp, E., Valentine, J. S., and Vila, A. J. (2000) *J. Am. Chem. Soc.* **122,** 3701–3707
66. Donaire, A., Jimenez, H. R., Moratal, J. M., De la Rosa, M. A., Hervas, M., Navarro, J. A., Monleon, D., Tejero, R., and Celda, B. (1998) *Inorg. Chim. Acta* **275,** 73–89
67. Bertini, I., Huber, J. G., Luchinat, C., and Piccioli, M. (2000) *J. Magn. Reson.* **147,** 1–8
68. Bertini, I., and Luchinat, C. (1996) in *NMR of Paramagnetic Substances* (Lever, A. B. P., ed) Vol. 150, Elsevier Science Publishers B.V., Amsterdam
69. Guiles, R. D., Basus, V. J., Sarma, S., Malpure, S., Fox, K. M., Kuntz, I. D., and Waskell, L. (1993) *Biochemistry* **32,** 8329–8340
70. Bertini, I., Eltis, L. D., Felli, I. C., Kastrau, D. H. W., Luchinat, C., and Piccioli, M. (1995) *Chemistry* **1,** 598–607
71. Banci, L., Bertini, I., Dikiy, A., Kastrau, D. H. W., Luchinat, C., and Sompornpisut, P. (1995) *Biochemistry* **34,** 9851–9858
72. Ubbink, M., Lian, L. Y., Modi, S., Evans, P. A., and Bendall, D. S. (1996) *Eur. J. Biochem.* **242,** 132–147
73. Boyd, J., Dobson, C. M., Morar, A. S., Williams, R. J. P., and Pielak, G. J. (1999) *J. Am. Chem. Soc.* **121,** 9247–9248
74. Tsan, P., Caffrey, M., Daku, M. L., Cusanovich, M., Marion, D., and Gans, P. (1999) *J. Am. Chem. Soc.* **121,** 1795–1805
75. Bertini, I., Luchinat, C., and Turano, P. (2000) *J. Biol. Inorg. Chem.* **5,** 761–764
76. Jeuken, L. J. C., Ubbink, M., Bitter, J. H., van Vliet, P., Meyer-Klaucke, W., and Canters, G. W. (2000) *J. Mol. Biol.* **299,** 737–755
77. Buning, C., Canters, G. W., Comba, P., Dennison, C., Leuken, L., Melter, M., and Sanders-Loehr, J. (2000) *J. Am. Chem. Soc.* **122,** 204–211
78. Vriend, G. (1990) *J. Mol. Graph.* **8,** 52–56
79. Banci, L., Bertini, I., Bren, K. L., Gray, H. B., Sompornpisut, P., and Turano, P. (1997) *Biochemistry* **36,** 8992–9001
80. Banci, L., Bertini, I., Gray, H. B., Luchinat, C., Reddig, T., Rosato, A., and Turano, P. (1997) *Biochemistry* **36,** 9867–9877
81. Banci, L., Bertini, I., Huber, R., Spyroulias, G., and Turano, P. (1999) *J. Biol. Inorg. Chem.* **4,** 21–31
82. Baistrocchi, P., Banci, L., Bertini, I., Turano, P., Bren, K. L., and Gray, H. B. (1996) *Biochemistry* **35,** 13788–13796
83. Englander, S. W., and Kallenbach, N. R. (1983) *Q. Rev. Biophys.* **16,** 521–655
84. Englander, S. W. (1992) *Science* **256,** 1684–1687
85. Bai, Y. W., Sosnick, T. R., Mayne, L., and Englander, S. W. (1995) *Science* **269,** 192–197
86. Milne, J. S., Mayne, L., Roder, H., Wand, A. J., and Englander, S. W. (1998) *Protein Sci.* **7,** 739–745
87. Baxter, S. M., and Fetrow, J. S. (1999) *Biochemistry* **38,** 4493–4503
88. Fetrow, J. S., and Baxter, S. M. (1999) *Biochemistry* **38,** 4480–4492
89. Barker, P. D., Bertini, I., Del Conte, R., Ferguson, S. T., Hajieva, P., Tomlinson, E., Turano, P., and Viezzoli, M. S. (2001) *Eur. J. Biochem.* 2001, **268,** 4468–4476
90. Dangi, B., Sarma, S., Yan, C., Banville, D. L., and Guiles, R. D. (1998) *Biochemistry* **37,** 8289–8302
91. Banci, L., Bertini, I., Cavazza, C., Felli, I. C., and Koulougliotis, D. (1998) *Biochemistry* **37,** 12320–12330
92. Arnesano, F., Banci, L., Bertini, I., and Felli, I. C. (1998) *Biochemistry* **37,** 173–184
93. Sari, N., Holden, M. J., Mayhew, M. P., Vilker, V. L., and Coxon, B. (1999) *Biochemistry* **38,** 9862–9871
94. Lyons, T. A., Ratnaswamy, G., and Pochapsky, T. C. (1996) *Protein Sci.* **5,** 627–639

Access the most updated version of this article at doi: 10.1074/jbc.M100304200

Alerts:
- When this article is cited
- When a correction for this article is posted

Click here to choose from all of JBC's e-mail alerts

Supplemental material:

http://www.jbc.org/content/suppl/2001/12/07/276.50.47217.DC1

This article cites 89 references, 4 of which can be accessed free at
http://www.jbc.org/content/276/50/47217.full.html#ref-list-1